A&A 566, A18 (2014)
DOI: 10.1051/0004-6361/201322978

Astronomy & Astrophysics

Discovery of weak 6.7 GHz CH_3OH masers in a sample of high-mass Hi-GAL sources*

L. Olmi[1,2], E. D. Araya[3], P. Hofner[4,**], S. Molinari[5], J. Morales Ortiz[2], L. Moscadelli[1], and M. Pestalozzi[5]

[1] INAF, Osservatorio Astrofisico di Arcetri, Largo E. Fermi 5, 50125 Firenze, Italy
e-mail: olmi.luca@gmail.com
[2] University of Puerto Rico, Rio Piedras Campus, Physics Dept., Box 23343, UPR station, San Juan, Puerto Rico, USA
[3] Physics Department, Western Illinois University, 1 University Circle, Macomb, IL 61455, USA
[4] New Mexico Institute of Mining and Technology, Physics Department, 801 Leroy Place, Socorro, NM 87801, USA
[5] Istituto di Fisica dello Spazio Interplanetario – INAF, via Fosso del Cavaliere 100, 00133 Roma, Italy

Received 4 November 2013 / Accepted 19 March 2014

ABSTRACT

Context. Maser lines from different molecular species, including water, hydroxyl, and methanol, are common observational phenomena associated with massive star-forming regions. In particular, since its discovery, the 6.7 GHz methanol maser has been recognized as one of the clearest signposts in the formation of young high-mass stars.

Aims. The methanol maser thus appears as an ideal tool for studying the early phases of massive star formation. However, it is difficult to establish the exact start of the methanol maser phase, and it would then be interesting to detect and study low flux-density methanol masers (i.e., $\lesssim$0.1 Jy or even $\ll$0.1 Jy), in order to determine if they can be used effectively to mark a specific evolutionary phase in high-mass star formation.

Methods. Past surveys have been unable to systematically detect many low flux-density methanol masers, and thus we do not yet know how many such masers exist in the Galaxy and what their physical nature is. A large sample of massive cores can now be found in the *Herschel* infrared GALactic Plane Survey (Hi-GAL), which we have used to search for methanol and excited OH masers toward a sample of starless and protostellar high-mass clumps using the Arecibo telescope.

Results. Out of a sample of 107 observed Hi-GAL sources, we detected a total of 37 methanol masers, with 22 sources being new and weak (median peak flux density 0.07 Jy) detections, in the Galactic longitude range [32°.0, 59°.8]. We also detected 12 6.035 GHz OH maser regions, with 9 new detections. Our survey covers a similar range of source distances to the "Arecibo Methanol Maser Galactic Plane Survey" (or AMGPS, Pandian et al. 2007), but the methanol masers detected by us are clearly shifted toward lower integrated flux densities.

Conclusions. The newly detected methanol masers mostly have low luminosity (assuming isotropic emission), and except for some sources, their weakness is not due to distance effects or positional offsets. No specific correlation is found with the physical parameters of the Hi-GAL clumps, except for sources with both CH_3OH and OH masers, which tend to have higher mass and luminosity. The intensity of the methanol masers correlates well with the velocity range of the maser emission, which suggests that the low brightness of these masers is related to the number of maser spots in the emitting region and to their evolution with time.

Key words. stars: formation – ISM: clouds – ISM: molecules

1. Introduction

Our current understanding of the formation process of intermediate to massive stars ($M \gtrsim 5\ M_\odot$) is limited by a combination of theoretical and observational challenges. On the theoretical side, the formation of massive stars is a highly complex process, which is also dependent on the interaction between the large-scale ($\gtrsim$10 pc) structure of molecular clouds/clumps and dynamic fragmentation properties during the prestellar phase.

On the observational side, only very recently has some progress been made toward identifying and studying the earliest phases of high-mass star formation (HMSF) and the transition from the high-mass starless core (HMSC) phase (the likely precursors of massive stars and clusters) to the high-mass protostellar object phase. However, the physical conditions in the HMSC and the exact evolutionary path from HMSC to massive stars are not well constrained.

Maser lines from different molecular species, including water, hydroxyl, and methanol, are common observational phenomena associated with massive star-forming regions. The relation between different types of masers found around young stellar objects may yield important information about the evolutionary state of the regions (e.g., Szymczak & Gérard 2004; Breen et al. 2010). In particular, since its discovery (Menten 1991), the 6.7 GHz methanol maser has been recognized as one of the clearest signposts in the formation of young high-mass stars. Theoretical models (e.g., Cragg et al. 2002) and observational studies (e.g., Ellingsen 2006) suggest that Class II methanol masers are exclusively associated with early phases of massive star formation. The methanol maser thus appears as an ideal tool for detecting a short-lived phase of HMSF, between the end of the large-scale accretion and the formation of massive protostars (Pestalozzi 2012). However, it is difficult to establish the

* Appendices are available in electronic form at http://www.aanda.org

** Adjunct Astronomer at the National Radio Astronomy Observatory.

exact start of the methanol maser phase and to study the physical properties in that phase.

A large sample of massive cores can now be found in the *Herschel* infrared GALactic Plane Survey (Hi-GAL), a key program of the *Herschel* Space Observatory to carry out a five-band photometric imaging survey at 70, 160, 250, 350, and 500 μm of a $|b| \leq 1°$-wide strip of the Milky Way Galactic plane (Molinari et al. 2010). This survey is now providing us with large samples of dust clumps in a variety of evolutionary stages and in various star-forming environments. With the main goal of determining the physical conditions in the Hi-GAL clumps and better understanding the evolutionary path of HMSCs toward massive stars, we have thus initiated an observing program at Arecibo with its own goal of determining whether a population of low flux-density masers exist and whether they can be used to mark a specific evolutionary phase in HMSF and/or a specific set of physical conditions.

2. Observations

2.1. Previous observations

During the past 10–15 years, extensive 6.7 GHz methanol maser searches have been undertaken using two different strategies: (1) targeted searches toward color-selected infrared sources and known regions of star formation (e.g., Walsh et al. 1997; Szymczak et al. 2002); and (2) unbiased surveys covering portions of the Galactic plane (for a summary see Green et al. 2009). In particular, the "Methanol Multibeam Survey" (MMBS, Green et al. 2009) will cover the whole Galactic plane in longitude and in a latitude range $|b| \leq 2°$ when completed. This survey also covers a previous smaller survey carried out at Arecibo (the "Arecibo Methanol Maser Galactic Plane Survey", or AMGPS, Pandian et al. 2007, 2011). All of these surveys have detected a total of about 800 masers in the range $\ell = 20°-186°$, but many more (∼1200–2500) are expected to be found (van der Walt 2005; Pestalozzi et al. 2007).

The targeted 1-σ noise level of the MMBS is ≤0.2 Jy (Green et al. 2008), whereas the AMGPS yielded an rms noise level of ∼70 mJy (Pandian et al. 2007). These are similar to the deepest previous unbiased surveys that had 1-σ sensitivities between 0.09 Jy and 1 Jy (see Pestalozzi et al. 2005). Pandian & Goldsmith (2007) find that the peak of the distribution of methanol masers as a function of flux density occurs between 0.9 and 3 Jy. They also find a turnover in the number of sources at lower flux densities, but they could not determine the shape of the distribution owing to their completeness limit of 0.27 Jy. (The completeness limit in the MMBS is ≈0.8 Jy.)

Therefore, these surveys have been unable to detect a significant number of *low flux-density* (i.e., $\lesssim$0.1 Jy or even ≪0.1 Jy) methanol masers, and thus we do not know yet how many such masers exist in the Galaxy and what their physical nature is. In particular, in light of the association of the 6.7 GHz methanol maser with the early stages of HMSF (e.g., Pestalozzi et al. 2002), it would be interesting to analyze whether low flux-density masers can be used effectively to mark a specific evolutionary phase in HMSF.

2.2. Selection of the source sample

The Hi-GAL survey offers the best opportunity for dealing with the issues described above, since it allows us to look at large clump populations in various clouds with different physical conditions, while using self-consistent analysis to derive their physical parameters (see, e.g., Elia et al. 2010, 2013; Olmi et al. 2013). Previous surveys suggest that methanol masers do not form toward low-mass molecular clumps. Therefore, the mass of the Hi-GAL clump can be used as the main selection parameter to help identify new methanol masers. Mass and other physical parameters of the Hi-GAL clumps were derived from a single-temperature spectral energy distribution (SED) model applied to suitable candidates in the Hi-GAL catalog. To extract candidate sources, a first catalog based on image photometry was compiled in each of the observed Hi-GAL fields, identifying the sources detected in the five different bands based on simple positional association. Correlations at multiple wavelengths were then used to construct the final catalog. (More details about this procedure will be published by Pestalozzi et al., in prep.)

For our observations at Arecibo, which were divided into three sessions (July 2012, January 2013, and May 2013), we observed a sample of 107 Hi-GAL sources using the following basic criteria: i) The targets had to be located in the inner Galaxy accessible to Arecibo. (We limited the range to $\ell \sim 30°-60°$.) ii) The sources had a mass $M > 10\ M_\odot$. (Since the true distance to these Hi-GAL sources had not been estimated yet, their preliminary masses were calculated using an arbitrary distance of 1 kpc.) iii) The sources must have been detected in all Hi-GAL bands longward of 70 μm. iv) For the sources observed during the January and May 2013 sessions, we also checked that they were not near (within 1 arcmin radius) any of the already known methanol masers. Given the observing restrictions at Arecibo, our selection criteria intentionally used only mass as main parameter in order to have a large enough sample of sources at our disposal.

2.3. Arecibo observations

The observations were conducted with the 305 m Arecibo Telescope[1] in Puerto Rico, between July 2012 and May 2013 as already mentioned. We used the C-Band High receiver to simultaneously observe the (5_1-6_0) transition of A^+ methanol at 6668.518 MHz and the 6035.092 MHz ($^2\Pi_{3/2} J = 5/2, F = 3-3$) excited-state OH line.

We used the WAPP spectrometer, full Stokes polarization setup, three-level sampling, 6.25 MHz (280 km s^{-1}) bandwidth, and 4096 channels per polarization, resulting in a channel separation of 1.53 kHz (0.068 km s^{-1}). We observed in ON-source (total power) mode, with integration times of five minutes, which yielded an rms noise level of ≃5–10 mJy in each spectral channel, depending on the smoothing level. Our sensitivity was thus much better than achieved in the MMBS and AMGPS surveys. The center bandpass LSR velocity was set to 70 km s^{-1}. The calibrator B2128+048 was observed in each run for pointing and system checking (1 min on-source observations). The pointing was typically better than 10″. We measured a telescope beam size of ∼42″ (at 6.6 GHz) and a typical gain of ∼6 K Jy^{-1}.

Data was reduced in IDL[2] using specialized reduction routines provided by the Arecibo Observatory. After checking for consistency, we subtracted low-order polynomial baselines.

[1] The Arecibo Observatory is operated by SRI international under a cooperative agreement with the National Science Foundation (AST-1100968) in alliance with Ana G. Méndez-Universidad Metropolitana and the Universities Space Research Association.

[2] http://www.exelisvis.com/ProductsServices/IDL.aspx

The spectra were imported to CLASS[3] for line parameter measurement and further analysis.

3. Results

3.1. Distance determination

Assigning a distance to sources detected with a photometer is a crucial step in giving physical significance to all information extracted from Hi-GAL data. While reliable distance estimates are available for a limited number of known objects (e.g., HII regions, see Russeil 2003, and masers, see e.g. Green & McClure-Griffiths 2011), this information does not exist for the majority of Hi-GAL sources. We adopted the scheme presented by Russeil et al. (2011) aiming to assign kinematic distances to large lists of sources: a ^{12}CO (or ^{13}CO) spectrum (e.g., from the BU-FCRAO Galactic Ring Survey, or GRS, Jackson et al. 2006) is extracted at the line of sight of every Hi-GAL source, and the VLSR of the brightest spectral component is assigned to it, allowing calculation of a kinematic distance (see details below). By using extinction maps (derived from the 2MASS point source catalog, see e.g. Schneider et al. 2011) and a catalog of sources with known distances (H II regions, masers, and others), the distance ambiguity is resolved and a recommendation given. In this way it is possible to produce a "distance map" having the same pixel size of the CO cube as used to extract the spectra for every target, where the value of the pixel is the assigned distance of the Hi-GAL source(s) falling in that pixel. The typical error on the kinematic distance[4] is estimated to vary between ~0.6–0.9 kpc in the range of longitude $\ell \sim 30°-60°$.

A source of error comes from using extinction maps to solve for the distance ambiguity. A comparison between distances to methanol maser sources assigned using extinction maps and HI self-absorption suggests that the former method tends to assign the far heliocentric distance more often (Pestalozzi et al., in prep.). The effects of this incorrect distance assignment are more severe, the larger the difference between near and far heliocentric distances, because of the square dependence of mass and luminosity on the source distance. For the present paper, however, we have to rely on the use of extinction maps for practical reasons, and also no spectral line emission has been observed for most of the sources other than what can be extracted from the GRS data cube (Jackson et al. 2006).

We also checked that there was some overlapping between our sample of Hi-GAL clumps and the sources observed in the BeSSeL Survey[5] ("Bar and Spiral Structure Legacy Survey", Brunthaler et al. 2011). We found only four methanol masers with a BeSSeL source within 5 arcmin (an additional source is within 12 arcmin), and in all these cases the distance determined by the BeSSeL team was *smaller* than what we determined with the method described above, by a factor 0.19 to 0.85 (see Reid et al. 2009). Clearly, if this trend is confirmed, it will make these masers even weaker (see Sect. 4.1).

3.2. New methanol and OH masers

Out of a sample of 107 observed Hi-GAL sources, we detected a total of 37 methanol masers (34% detection rate), whose spectra are shown in Fig. A.1, in the Galactic longitude range [32°.0, 59°.8]. We also detected 12 6.035 GHz OH masers (11% detection rate), with nine objects that are new detections (see Fig. B.1). The J2000.0 positions, velocity range of maser emission $[V_{min}, V_{max}]$, peak flux density, S_{pk}, integrated flux density, $\int S\, dV$, and the estimated distance, d, for each source are given in Tables 1 and 2 for the methanol and OH masers, respectively. Table C.1 lists the Hi-GAL sources where no methanol maser was detected, and we report the rms of the final spectrum for each source. As shown in Table 1 some nearby Hi-GAL sources may not be observed as separated objects through the Arecibo beam and sidelobes. Therefore, when counting the *new* methanol masers, we have excluded the detections toward sources G32.14+0.13, G33.59-0.03, G33.65-0.02, and G41.13-0.19. Thus we are left with 22 effectively new detections instead of the 26 sources listed in Table 1. Only one of the newly detected methanol masers (G34.71-0.59) has an associated OH maser.

The positions of the new detected methanol and OH masers are graphically shown in the top panel of Fig. 1, where a higher concentration of sources is clearly seen around $\ell \simeq 35°$ and $b \simeq 0°$, where giant molecular clouds can be found that contain the W44 supernova remnant (e.g., Reach et al. 2005). We note that a total of seven maser sources are found outside the galactic latitude range $|b| \leq 0°.5$, which was explored by the AMGPS survey. We also note that Green et al. (2010) find that 97% of their MMBS sources are at a latitude within 1° of the Galactic plane.

As a comparison, Fig. 1 also shows the positions of the UC H II regions, a typical signpost of HMSF, from the CORNISH catalog (Hoare et al. 2012; Purcell et al. 2013). One can note that the methanol masers follow the general distribution of the UC H II regions, and in some cases their positions are clearly coincident. In fact, we find that seven methanol masers have a UC H II region within 45 arcsec (i.e., about one Arecibo beam). Three of these masers (G32.74-0.07, G33.13-0.09, and G33.41-0.00) were already known (see Table 1), whereas the other four are new and low flux-density masers (G34.19-0.59, G35.46+0.13, G35.57-0.03, and G37.86-0.60). Although the nature of this association will have to be further investigated through higher-angular resolution observations, we see that most of our newly detected methanol masers do *not* have an associated UC H II region (at the sensitivity level of the CORNISH catalog). This result suggests that masers like these are more likely associated with the *pre*-UC H II phase of HMSF.

The bottom panel of Fig. 1 shows the longitudes and velocities of all maser sources detected at Arecibo. Since 6.7 GHz methanol masers are only detected toward regions of HMSF, they are expected to be found within spiral arms. We find that the median (mean) velocity of all masers (methanol and OH) is 60.0 ± 20.7 km s^{-1} (61.9 ± 20.8 km s^{-1}). Five sources have velocities lower than 30 km s^{-1}, while there is only one source with a velocity exceeding 120 km s^{-1}. By comparison with the velocity-longitude plot of Pandian et al. (2007), we can see that we have a main group of sources, with $\ell \sim 35°$ to 40° and $V_{lsr} \sim$ 60 km s^{-1} to 80 km s^{-1}, which fall near the Carina-Sagittarius arm. Another, less numerous group of sources can be found near the overlapping region between the Carina-Sagittarius and Perseus arms. We also note that a significant fraction of the masers do not lie near any spiral arm loci, a phenomenon already discussed by Pandian & Goldsmith (2007) and Green et al. (2010). This fact may be related with the results of Reid et al. (2009), who find that on average the HMSF regions orbit the Galaxy ≈15 km s^{-1} slower than the Galaxy spins.

[3] CLASS is part of the GILDAS software package developed by IRAM.

[4] This estimate assumes that the distance ambiguity has been correctly solved.

[5] http://www3.mpifr-bonn.mpg.de/staff/abrunthaler/BeSSeL/

Table 1. 6.7 GHz methanol masers detected with the Arecibo telescope.

Name	RA [J2000.0]	DEC [J2000.0]	V_{min} [km s^{-1}]	V_{max} [km s^{-1}]	S_{pk} [Jy]	$\int S_\nu dV$ [Jy km s^{-1}]	Nearest source	Ang. separ. [arcsec]	d [kpc]	New?	Ref.[a]
G32.14+0.13	18:49:32.5	–00:38:09	92.3	93.2	0.03	1.1E-02	G32.11+0.09	189	6.1	Y	–
G32.11+0.09	18:49:37.7	–00:41:00	90.2	104.5	1.2	7.7E-01	G32.14+0.13	189	5.2[b]	N	S1999
G32.74-0.07	18:51:21.8	–00:12:05	24.1	47.9	48	1.1E+02	–	–	2.5	N	CAS1995
G33.09+0.06	18:51:30.5	00:10:41	77.9	84.9	0.14	9.2E-02	–	–	5.3	Y	–
G32.82-0.08	18:51:32.1	–00:07:51	58.4	60.3	0.05	3.7E-02	–	–	5.9	Y	–
G33.13-0.09	18:52:07.9	00:08:13	70.4	82.2	11	1.5E+01	–	–	4.9	N	SHK2000
G33.41-0.00	18:52:20.1	00:25:47	97.0	108.2	0.43	8.3E-01	–	–	–	N	SHK2000
G33.59-0.03	18:52:46.0	00:34:09	102.6	103.5	0.02	1.4E-02	G33.61-0.03	107	–	Y	–
G33.61-0.03	18:52:49.0	00:35:46	102.8	103.8	0.07	5.2E-02	G33.59-0.03	107	6.5[b]	Y	–
G33.65-0.02	18:52:50.2	00:37:40	101.6	103.7	0.06	4.1E-02	G33.61-0.03	114	4.5	Y	–
G34.37+0.23	18:53:13.6	01:23:31	54.9	63.7	1.6	9.9E-01	–	–	1.6[b]	N	SHK2000
G34.08+0.01	18:53:30.5	01:02:03	54.7	61.6	0.73	5.5E-01	–	–	3.7	N	SKH2002
G35.46+0.13	18:55:34.2	02:19:11	73.2	74.4	0.02	1.4E-02	–	–	5.1	Y	–
G34.19-0.59	18:55:51.2	00:51:18	57.6	63.1	0.22	1.8E-01	–	–	3.8	Y	–
G35.57-0.03	18:56:22.6	02:20:28	127.0	127.6	0.02	6.0E-03	–	–	10.4	Y	–
G34.71-0.59	18:56:48.2	01:18:46	77.8	80.0	0.01	4.0E-03	–	–	–	Y	–
G35.13-0.74	18:58:06.0	01:37:06	26.1	40.8	32	3.5E+01	G35.14-0.75	62	2.2[b]	N	SHK2000
G35.14-0.75	18:58:09.9	01:37:27	26.2	39.4	1.7	1.8E+00	G35.13-0.74	62	2.3	N	SHK2000
G36.42-0.16	18:58:23.2	03:02:11	71.4	72.3	0.03	1.1E-02	–	–	8.6	Y	–
G36.83-0.02	18:58:39.0	03:28:00	52.7	64.5	2.5	6.4E+00	–	–	3.9	N	PGD2007[c]
G37.04-0.03	18:59:04.2	03:38:34	77.9	86.5	9.6	1.8E+01	–	–	5.6	N	P2011
G37.34-0.06	18:59:43.1	03:53:39	51.3	52.6	0.02	1.5E-02	–	–	9.8	Y	–
G37.19-0.41	19:00:43.4	03:36:24	29.4	30.1	0.07	2.3E-02	–	–	11.1	Y	–
G37.86-0.60	19:02:36.0	04:07:03	49.3	54.2	0.19	2.5E-01	–	–	3.4	Y	–
G38.93-0.36	19:03:42.0	05:10:23	31.0	33.8	0.04	4.6E-02	–	–	2.7	N	SHK2000, PGD2007
G39.99-0.64	19:06:39.9	05:59:13	71.5	72.1	0.02	5.0E-03	–	–	4.3	Y	–
G41.13-0.19	19:07:10.2	07:12:16	55.6	63.8	0.03	1.4E-02	G41.16-0.18	106	4.3	Y	–
G41.16-0.18	19:07:11.2	07:14:02	55.6	63.6	0.07	8.1E-02	G41.13-0.19	106	4.2	Y	–
G41.05-0.24	19:07:12.4	07:06:25	65.0	65.7	0.12	4.3E-02	–	–	8.1	Y	–
G43.10+0.04	19:09:59.7	09:03:58	8.8	10.1	0.02	1.9E-02	–	–	11.1[b]	Y	–
G43.53+0.01	19:10:52.9	09:25:44	51.6	52.9	0.09	2.8E-02	–	–	–	Y	–
G47.04+0.25	19:16:41.5	12:39:19	101.5	102.0	0.02	3.5E-03	–	–	4.7	Y	–
G45.87-0.37	19:16:42.9	11:19:10	59.6	60.5	0.02	1.1E-02	–	–	5.2	Y	–
G46.32-0.25	19:17:09.0	11:46:24	41.5	41.9	0.02	5.0E-03	–	–	7.4	Y	–
G56.96-0.23	19:38:16.8	21:08:07	29.3	30.6	1.1	4.2E-01	–	–	3.0	Y	–
G59.78+0.63	19:41:03.0	24:01:15	36.2	40.6	0.03	2.7E-02	–	–	2.1	Y	–
G59.63-0.19	19:43:49.9	23:28:37	21.9	32.8	0.58	5.1E-01	–	–	2.3	Y	–

Notes. Source names in boldface indicate an OH maser counterpart determined using both positional and velocity association criteria (see Table 2). V_{min} and V_{max} are the minimum and maximum velocity corresponding to the range of emission of the maser. S_{pk} is the peak flux density, and $\int S\, dV$ is the integrated flux density in the velocity range [V_{min}, V_{max}]. The 8th and 9th columns show the nearest Hi-GAL source (if the angular separation is ≤200 arcsec) for crowded fields, and the corresponding angular separation. In this case they are either the same source or there is likely some contamination from the sidelobes. d is the estimated distance of the Hi-GAL source (the typical error on the distance is ~0.6–0.9 kpc). The 11th column indicates whether the maser is a new detection (Y) or a known source (N). [(a)] S1999, Slysh et al. (1999). CAS1995, Caswell et al. (1995). SHK2000, Szymczak et al. (2000). SKH2002, Szymczak et al. (2002). PGD2007, Pandian et al. (2007). P2011, Pandian et al. (2011). [(b)] Distance determined from the BeSSeL Survey (see Sect. 3.1). [(c)] The RA of this source is incorrectly reported by PGD2007, but it is listed correctly by P2011.

Table 2. Same as Table 1 for the 6.0 GHz OH masers detected with the Arecibo telescope.

Name	RA [J2000.0]	Dec [J2000.0]	V_{min} [km s^{-1}]	V_{max} [km s^{-1}]	S_{pk} [Jy]	$\int S_\nu dV$ [Jy km s^{-1}]	d [kpc]	New?
G32.74-0.07	18:51:21.8	–00:12:05	25.1	39.2	0.56	0.978	2.5	N
G33.70+0.28	18:51:50.4	00:49:06	24.3	26.0	0.03	0.029	2.6	Y
G33.13-0.09	18:52:07.9	00:08:14	72.2	79.9	0.04	0.037	4.9	N
G34.13+0.07	18:53:21.3	01:06:11	62.1	62.2	0.02	0.006	3.8	Y
G35.74+0.15	18:56:01.0	02:34:34	81.8	85.8	0.02	0.031	5.6	Y
G35.57-0.03	18:56:22.6	02:20:28	81.1	87.0	0.04	0.086	10.4	N
G34.71-0.59	18:56:48.2	01:18:46	81.8	85.0	0.02	0.031	–	Y
G35.13-0.74	18:58:06.0	01:37:07	32.8	37.1	3.92	3.615	2.2	Y
G37.81+0.41	18:58:53.9	04:32:15	18.1	18.4	0.04	0.009	1.2	Y
G35.29-0.89	18:58:57.0	01:41:40	57.6	58.5	0.04	0.019	2.5	Y
G37.04-0.03	18:59:04.2	03:38:34	81.1	85.1	0.05	0.073	5.6	Y
G59.63-0.19	19:43:49.9	23:28:37	66.7	67.2	0.01	0.004	2.3	Y

Notes. Source names in boldface indicate a methanol maser counterpart (see Table 1).

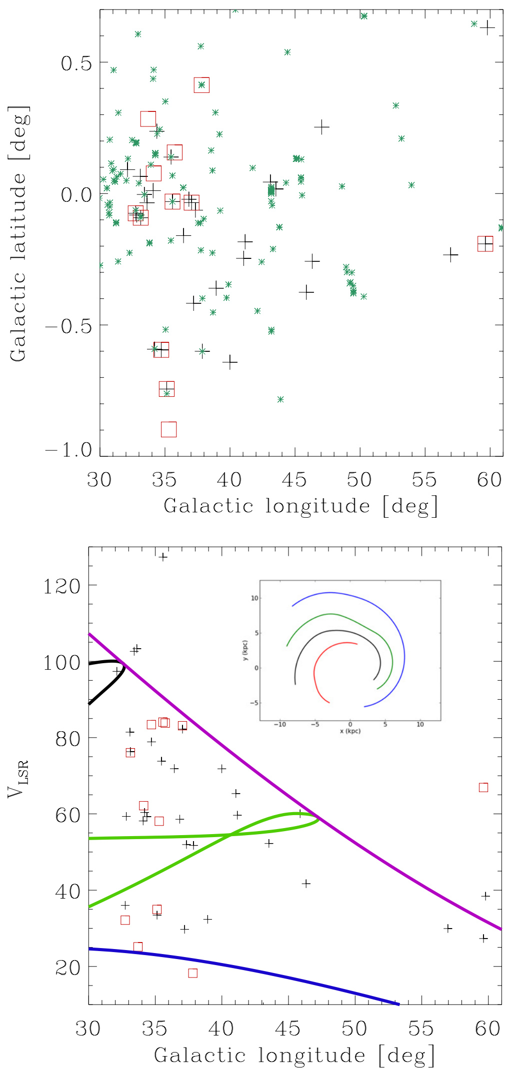

Fig. 1. *Top panel*. Region searched for maser counterparts to Hi-GAL sources. Methanol maser detections are denoted by "+" signs, and OH maser detections by red squares. Also shown are the UC H II regions from the CORNISH catalog (green asterisks). The concentration of sources around $\ell \simeq 35°$ and $b \simeq 0°$ is near the W44 region. *Bottom panel*. Longitude-velocity distribution of all masers detected at Arecibo. The colored loci represent the spiral arms and correspond to those shown in the inset: Norma (red), Scutum (black), Sagittarius (green), Perseus (blue). The locus of the tangent point is shown in purple.

Figure A.1 shows that the spectra of the masers are composed of many spectral features spread over a range of velocities. The total velocity spread in an individual source depends on the sensitivity of the observation, particularly when attempting to observe weak masers, and may also change as a result of the intrinsic variability of the components. The median (mean) spread in velocity for the methanol and OH masers, respectively, is 2.8 km s^{-1} (5.4 km s^{-1}) and 3.1 km s^{-1} (5.0 km s^{-1}). A wide velocity range ($\gtrsim$15–20 km s^{-1}) may also be caused by different maser sources falling within the Arecibo beam. For example, the methanol maser source G32.82-0.08 has a component near 60 km s^{-1} and another near 30 km s^{-1}, yielding a velocity range of about 23 km s^{-1}. However, the only new maser component is the one at higher velocity, whereas the component at $\simeq$30 km s^{-1} is likely to be contamination from the known methanol maser G32.74-0.07, which itself has a wide velocity range. Another example of contamination in the beam is described in the next section.

3.3. Cross scans and long-integration observations

During our observations at Arecibo we selected several sources (see Table 3) to perform a cross-scan centered on the nominal Hi-GAL position and with 24 arcsec (about half beam) angular steps. Table 3 shows the results obtained at various dates, and in the case of source G41.16-0.18, it also shows that different offsets were obtained depending on the *velocity component* used for the computation (see Fig. 2). This is clearly an indication that distinct spatial maser components were simultaneously present within the Arecibo beam, which can only be shown during a cross scan. The results listed in Table 3 show that in most cases the maser was observed within the main beam, and the estimated offset was less than or comparable to the Arecibo telescope pointing errors ($\lesssim$15 arcsec, see Sect. 2.3), except on June 5, 2013, when the estimated offset was quite large.

An interesting question is whether multiple velocity maser components are more prevalent in high-flux density maser sources or not (see Sect. 4.6). Therefore, in a few selected low flux-density masers (G45.87-0.37, G43.53+0.01, G59.78+0.63), we performed several consecutive 5 min scans (totalling 15–25 min integration time), which we then averaged in order to check for multiple maser components that could have escaped the single 5 min integrations because of sensitivity limitations. The selected sources all initially appeared to have a

Table 3. Results of cross scans performed at Arecibo.

Source	Date observed	Velocity component [km s^{-1}]	ΔRA [arcsec]	ΔDec [arcsec]	Total offset [arcsec]
G37.86-0.60	26-Jan.-2013	51.1	−0.7	2.0	2.2
G56.96-0.23	21-Jan.-2013	29.8	8.2	8.8	12.0
G41.16-0.18	30-May-2013	56.0	6.8	4.1	7.9
G41.16-0.18	30-May-2013	62.8	0.7	−2.7	2.8
G41.05-0.24	30-May-2013	65.4	8.5	−11.1	13.9
G59.63-0.19	31-May-2013	29.6	0.8	−6.0	6.0
G59.78+0.63	31-May-2013	38.3	11.9	14.5	18.7
G45.87-0.37	05-Jun.-2013	59.9	22.1	17.0	29.9

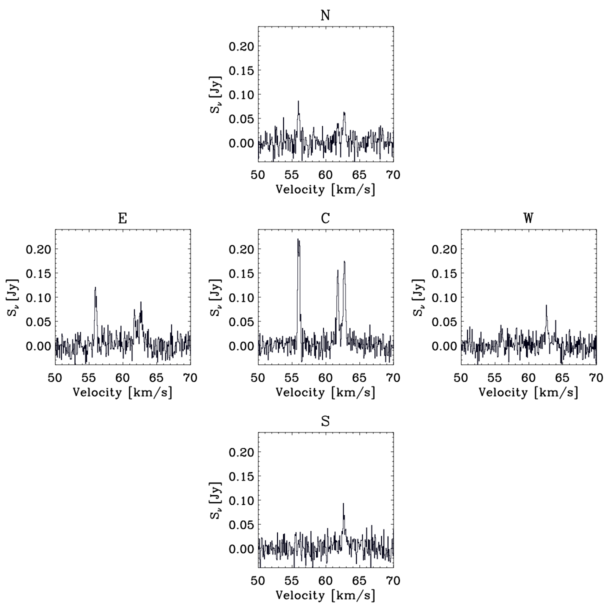

Fig. 2. Cross scan (with 24 arcsec angular step) performed on source G41.16-0.18, showing different velocity components and their variation as a function of position.

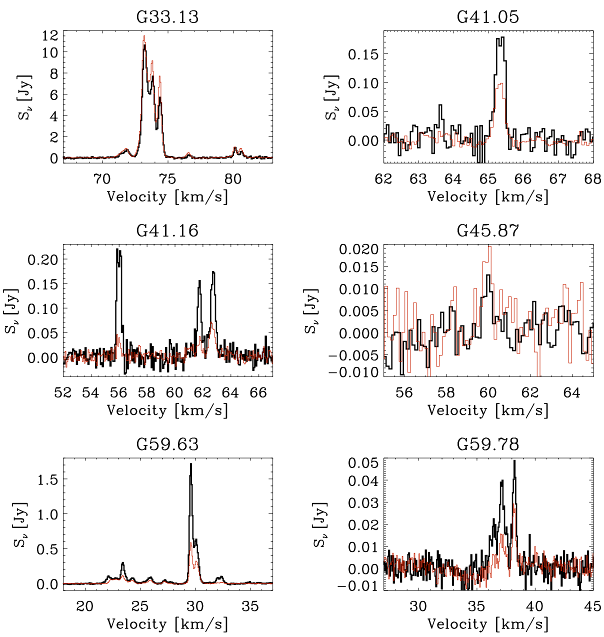

Fig. 3. Spectra of methanol masers observed on different dates, with the red (thin) and black (thick) solid lines representing older and more recent spectra, respectively.

single-component spectrum (G45.87-0.37, G43.53+0.01) or had just a few components occupying a narrow ($\lesssim$5 km s^{-1}) range of velocities (G59.78+0.63). Our long-integration spectra of these sources did *not* show any new component.

In addition to sensitivity, another possible explanation for the non-detection of multiple velocity components is that the source is being observed off-peak, leaving only the most intense component detectable. In this regard we note that sources G45.87-0.37 and G59.78+0.63 were also observed in cross-scan mode, as described in the previous section and in Table 3. Therefore, the long-integration scans were performed toward the observed peak position of the five-pointing cross scans. The observed peak positions turned out to be very close to the estimated actual positions of the sources. Despite this adjustment, we still did not observe any additional velocity component. This test toward a very small number of sources is neither complete nor conclusive, and more sensitive observations toward a larger sample of low flux-density methanol masers are clearly needed to confirm this trend. However, we can use this result as a tentative indication that the weak methanol masers detected at Arecibo do indeed tend to have fewer velocity components than previously observed brighter masers (see also Sect. 4.3).

3.4. Variability

To test the variability of the methanol masers detected by us, we observed some of the sources on different dates, and we selected both weak and relatively bright masers. In Fig. 3 we show the methanol spectra observed on at least two different dates (e.g., July 2012 or January 2013, and May or June 2013). The sources showing the greatest variation in intensity are G41.16-0.16, G59.63-0.19, G59.78+0.63, and to a lesser degree, G41.05-0.24. The other sources show variations $\lesssim$20% (see Table 4), which could be accounted for by calibration and pointing uncertainties.

In sources G33.13-0.09 and G41.16-0.16, we note the greatest difference between the variation of the peak flux density and the total flux integrated over all velocity components. Thus, not all of the observed maser components have varied by the same amount during the period considered, either because they vary differently with time, or because they do not belong to the same source. In the specific case of G41.16-0.16, given the results of the cross scan performed on this source (Sect. 3.3), we favor the second alternative.

Table 4. Variability of a few selected methanol masers.

Source	Initial date observed	Final date observed	Velocity component [km s^{-1}]	Flux density variation [%]	Flux variation [%]
G33.13-0.09	July 2012	May 2013	73.3	−8	−17
G41.05-0.24	July 2012	May 2013	65.4	42	35
G41.16-0.18	January 2013	May 2013	56.0	380	135
G43.10+0.04	January 2013	May 2013	9.5	9	8
G45.87-0.37	January 2013	May 2013	60.0	−32	−33
G59.63-0.19	July 2012	May 2013	29.6	202	159
G59.78+0.63	July 2012	May 2013	38.3	96	107

Notes. Columns 5 and 6 list the percentage difference in the peak flux density (at the velocity indicated in Col. 4) and of the total flux between the initial and final dates of observation.

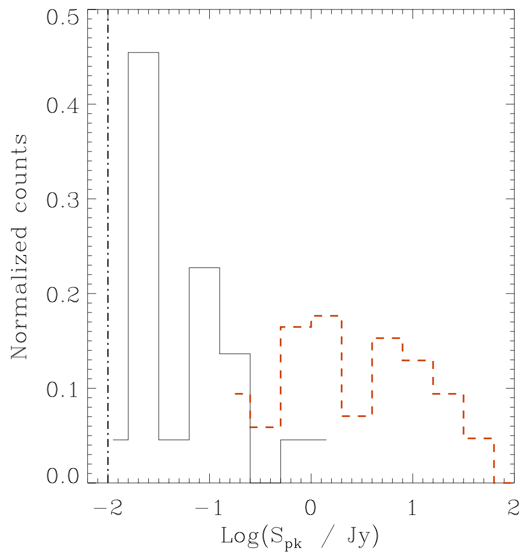

Fig. 4. Normalized counts (number of sources per bin divided by the total number of sources) vs. peak flux for the new methanol masers detected at Arecibo (black solid line) and for the AMGPS (Pandian et al. 2007, 2009; red dashed line). The rms noise level in our spectra was ~5–10 mJy (shown by the dash-dotted vertical line) in each spectral channel (see Table C.1).

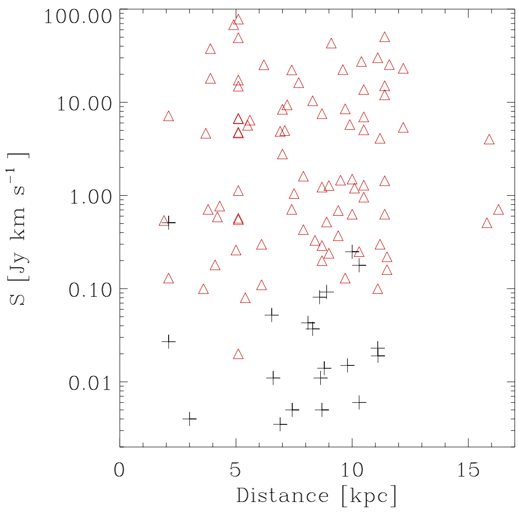

Fig. 5. Methanol maser flux vs. distance of the associated clump for all masers found by Pandian et al. (2007) (red triangles) and our *newly detected* methanol masers (black "+" signs). The median value of the integrated flux density of our own masers is ≃0.03 Jy km s^{-1}, while the median value for the AMGPS masers is ≃1.6 Jy km s^{-1}.

4. Discussion

4.1. Intrinsic maser intensity

As mentioned in Sect. 2.1, Pandian & Goldsmith (2007) found that the maximum of the distribution of their methanol masers as a function of flux density occurred for peak flux densities between 0.9 and 3 Jy. Figure 4 shows that the peak flux density distribution of the 6.7 GHz methanol masers detected toward our sample of Hi-GAL sources does not follow the distribution found by Pandian & Goldsmith (2007). This is not surprising since our sensitivity is better than in previous surveys, and we have excluded already known strong methanol masers from our analysis.

But, clearly the interesting question is whether the *intrinsic* intensity of these masers is also lower than that of previously known methanol masers. In fact, the simplest explanation of the weakness of our masers would be that, for example, most sources in our Hi-GAL sample are systematically more distant than the sources observed by Pandian et al. (2007). However, we can exclude this observational selection effect because Fig. 5 clearly shows that although both source samples approximately cover the same distance range, the AMGPS masers are clearly shifted toward higher integrated flux densities, with a median value that is about 50 times higher than that of our sample. In addition, we have seen in Sect. 3.1 that where a BeSSeL counterpart exists, its distance is less than what we determined.

Another possibility for explaining the difference shown in Fig. 5 would be to assume that the low brightness of our sources is caused by the masers being systematically offset with respect to the nominal position of the Hi-GAL source, or even by observing a known methanol maser in a sidelobe of the Arecibo beam. It seems very unlikely that *all* of the weak masers detected by us have been observed with such a large pointing offset to fully justify their lower intensity. In fact, the cross scans discussed in Sect. 3.3 and listed in Table 3 show that the typical measured offset may account for at most a ≃25% decrease in the maser peak intensity and thus cannot justify the difference of about a factor of 50 between the median values of the integrated flux densities previously mentioned.

Figure 6 indeed suggests that our methanol masers are intrinsically weaker than those detected in the AMGPS. In the top panel, the normalized histogram of the peak flux density multiplied by the distance squared, $S_{\rm pk} \times d^2$, shows a pronounced peak at low values for our methanol masers. Given that the AMGPS and our samples have a similar number of sources, we

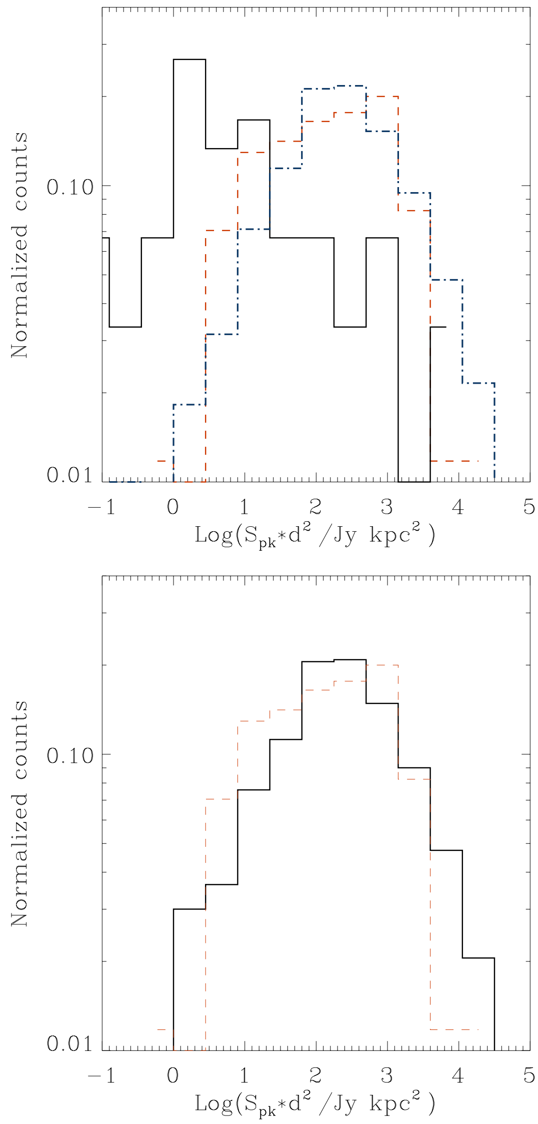

Fig. 6. *Top panel*: normalized counts (number of sources per bin divided by the total number of sources) vs. $S_{\rm pk} \times d^2$, for the Pandian et al. (2007, 2009) data (red dashed line), the MMBS masers exclusively associated with Hi-GAL sources (dot-dashed blue line), and our own results (solid black line), including new and known methanol masers. *Bottom panel*: normalized counts vs. $S_{\rm pk} \times d^2$ of the merged distributions of the Hi-GAL MMBS masers with our own masers (black, solid line), and the AMGPS (dashed red line).

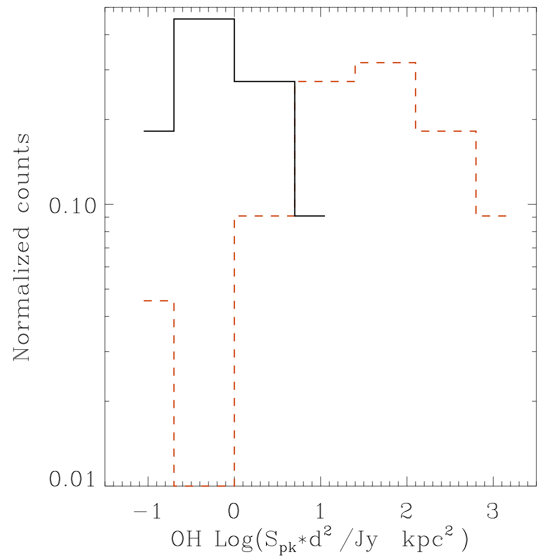

Fig. 7. Normalized counts (number of sources per bin divided by the total number of sources) vs. $S_{\rm pk} \times d^2$ of the OH masers, for both the Caswell & Vaile (1995) data (dashed red line) and our own results (solid black line). The bin width has been increased compared to Fig. 6.

do not expect statistical fluctuations to affect this comparison. We also note that the lowest bins of the AMGPS may be affected by completeness (Pandian et al. 2009), whereas our distribution is robust even in the lowest bins, since it is a pointed survey. Figure 6 also allows comparing the distributions of all AMGPS masers and of the MMBS masers exclusively associated with Hi-GAL sources (in the ranges $\ell = 0°{-}20°$ and $\ell = 290°{-}360°$, publicly available), which appear quite similar. In addition, if we merge the $S_{\rm pk} \times d^2$ distribution of the MMBS with ours and compare the result with the AMGPS, Fig. 6 shows that the merged distribution has an excess at the low end owing to the contribution of the low flux-density masers we found. Therefore, while Hi-GAL sources in general do not show a markedly different $S_{\rm pk} \times d^2$ distribution compared to the AMGPS blind survey, our sample does fall at the low end of this distribution.

Figure 7 represents a similar plot to the one shown in Fig. 6, but for the excited OH masers. In this case the comparison is done with the survey of Caswell & Vaile (1995). In Fig. 6 the distribution of the methanol masers we detected clearly has its peak shifted toward lower values of $S_{\rm pk} \times d^2$, compared to the reference distribution. Figure 7 also suggests a similar shift to lower intensities for our OH masers, but given the much lower number of detections, this cannot be considered a firm conclusion yet. Figures 6 and 7, however, both indicate that our blind survey toward Hi-GAL sources was indeed more sensitive to the low-intensity tail of the distribution of methanol and OH maser intensities.

4.2. Masers luminosity function

Using the kinematic distance one can also calculate the isotropic luminosities of the masers (using their integrated flux densities, S) and the methanol maser luminosity function. In this regard we briefly discuss the completeness of our sample of massive Hi-GAL clumps observed at Arecibo. If we use the completeness limits, in terms of flux density, determined by Elia et al. (2013), a dust temperature of 15 K, a dust emissivity index $\beta = 2$, and dust mass absorption coefficient $k_{250} = 10$ cm^2 g^{-1}, then the mass completeness limit at a distance of 10 kpc turns out to be $\sim$50 $M_\odot$. Since most of the clumps in our sample have masses above this limit, completeness effects should be negligible.

The top panel of Fig. 8 shows the luminosity function of 6.7 GHz methanol masers, compared with the luminosity function of the AMGPS masers (Pandian et al. 2009). In this case we do not show a comparison with the MMBS because the luminosity function could not be calculated since the masers' integrated flux densities were not available. An interesting feature of Fig. 8 is that the peak of our distribution overlaps nicely with the bins of the AMGPS distribution, which may be affected by completeness effects. Therefore, in the bottom panel of Fig. 8 we plot the distribution obtained by merging our sample with the AMPGS masers. We note that since the counts at luminosities $L < 10^{-7}$ $L_\odot$ come mainly from our data, they are not affected by completeness effects, and thus the turnover at low luminosities

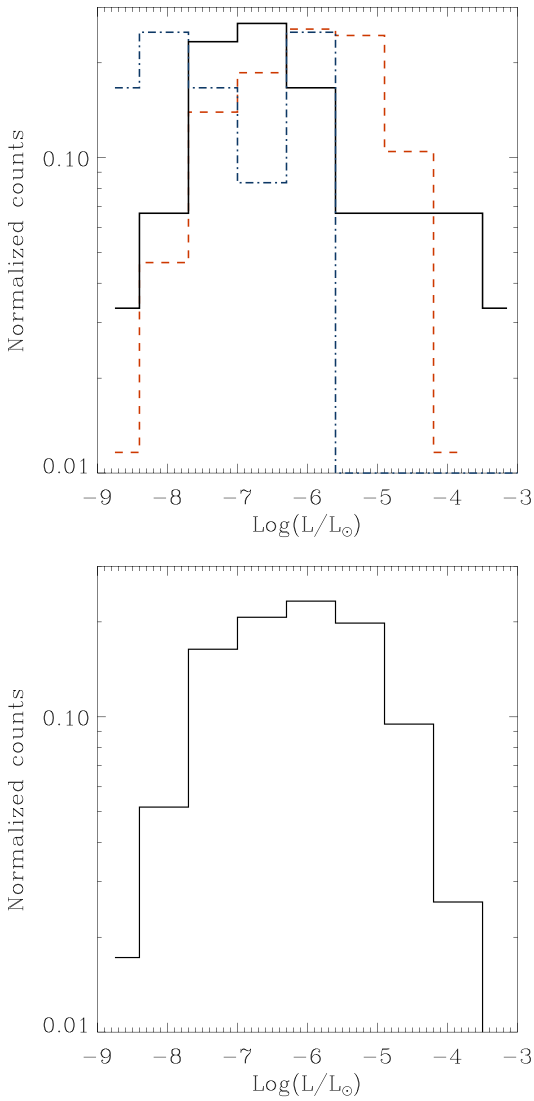

Fig. 8. *Top panel*: normalized counts (number of sources per bin divided by the total number of sources) vs. luminosity of the methanol masers, for both the Pandian et al. (2007, 2009) data (red dashed line) and our own results (including new and known masers) with the luminosity of both the methanol (black solid line) and OH masers (blue dash-dotted line). *Bottom panel*: normalized counts vs. luminosity of all methanol masers from both our survey and the AMGPS.

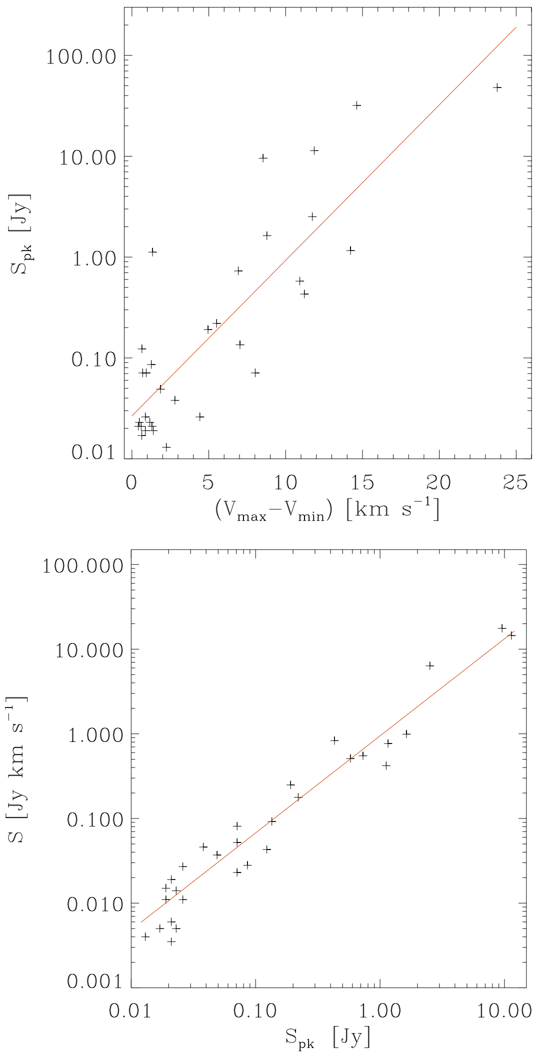

Fig. 9. *Top panel*: peak flux density of the methanol masers vs. the difference between the maximum and minimum values of the velocity range of emission. The solid line represents the linear fit (from Bayesian statistics, see text) to all points. The Spearman rank coefficient is 0.75. *Bottom panel*: flux of the methanol masers vs. the peak flux density. The solid line also represents the linear fit, and the Spearman rank coefficient is 0.96.

(but still higher than the minimum measured luminosity) is real. Figure 8 also shows the luminosity function of the 6.0 GHz OH masers, which is more uncertain due to the low number of OH masers detected. The range of OH luminosities is similar to that of the methanol masers, but no other trend is visible, and a more detailed comparison with the luminosity function of the methanol masers cannot be done with these data alone.

While the luminosity functions and the distributions of the $S_{\rm pk}\times d^2$ parameter bear some resemblance, they are not expected to be exactly the same, since the latter do not take the linewidths and multiple emission components into account. The luminosity of the maser emission is supposed to be a more reliable indicator of the physical conditions in a region since it depends on the conditions over a larger gas volume and will be less influenced by the fluctuations responsible for the intensity of a single spectral peak. On the other hand, one might also think that the intrinsic sensitivity of the quantity $S_{\rm pk}\times d^2$ to the main (or single) component of the maser emission would make this parameter better suited for a comparison of the relative strength between our maser sample and the AMGPS masers.

For example, this might be the case if the luminosity of the weak masers ($S_{\rm pk} \ll 1$ Jy) were systematically underestimated because the sensitivity of the observations is not good enough to detect all multiple emission components. The top panel of Fig. 9 would appear to support this assumption, since the masers with the lowest $S_{\rm pk}$ are also characterized by a lower velocity range, or actually show only one emission component. However, the bottom panel of Fig. 9 shows that the flux is well correlated with the peak flux density, thus indicating that the flux is indeed dominated by the brightest maser velocity component. In both cases we used the Bayesian IDL routine LINMIX_ERR to perform a linear regression to find the slope of the best fit line.

4.3. Properties of associated Hi-GAL clumps

Previous works have already attempted to find possible correlations between the physical parameters of the gas/dust clump

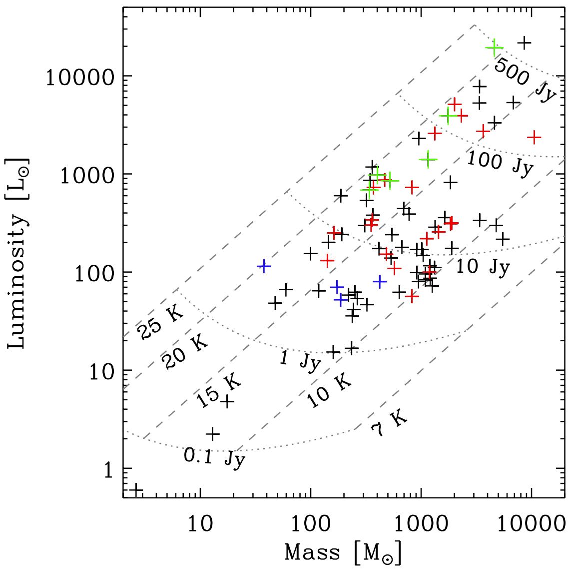

Fig. 10. Luminosity versus mass for all clumps (black "+" signs) observed at Arecibo, estimated using the distances listed in Table 1. Sources where a methanol or OH maser has been detected are shown in red and blue, respectively; sources with both masers are shown in green (both newly detected and previously known masers are shown). The dashed lines are loci at constant T = 10, 20, 30, and 40 K. Roughly orthogonal to these are loci (dotted lines) of constant 250 μm flux density, ranging from 0.1 to 500 Jy (assuming a modified blackbody spectral energy distribution with β = 1.5 and a fixed, "typical" distance of ~6 kpc).

where maser activity is present and, for example, the luminosity of the maser emission. Breen et al. (2010), among others, find that the 1.2 mm dust clumps with associated methanol masers have higher values of mass and radius than those with no associated 6.7 GHz methanol maser.

In Fig. 10 we present a luminosity vs. mass plot of all the Hi-GAL sources observed by us at Arecibo for which luminosity and mass could be calculated. These two physical parameters were determined using the estimated distance to the sources (see Sect. 3.1) and using a simple, single-temperature (SED) model to fit the PACS and SPIRE flux densities. Therefore, both luminosity and mass refer to the cold ($T_{\rm d} \lesssim$ 20–30 K) dust envelope of the Hi-GAL clumps (and should therefore be indicated as $M_{\rm env}$ and $L_{\rm env}$), and may be insensitive to warmer dust (emitting mostly shortward of ~24 μm) if a central protostar (or cluster of protostars) has already formed within the clump.

In Fig. 10 one should thus be aware that the envelope luminosities may be *underestimating* the total (i.e., bolometric) clump luminosity, $L_{\rm bol}$, if both warm and cold dust components exist within the Hi-GAL clump. With this *caveat*, in this figure we then show the groups of sources associated with a methanol or OH (or both) maser in different colors. It can be noted that while sources with only a methanol maser associated do not show any recognizable distribution pattern, sources with either just an OH maser or with both masers seem to occupy different regions in this plot. Hi-GAL clumps where *both* masers have been detected do show somewhat higher masses and luminosities. However, given our low number of sources and that the internal structure of the Hi-GAL clumps is not yet known, these trends are not statistically significant.

Likewise, for these weak masers we are unable to find any evidence of the trends discussed by Breen et al. (2010). We note that their analysis is based on the data by Hill et al. (2005), whose angular resolution is comparable to that of the Hi-GAL maps. We have also estimated the gas density in the observed Hi-GAL clumps, with and without an associated methanol maser. The results are plotted in Fig. 11, which shows that no significant difference is observed between the distributions of sources with and without a maser. These results are not too surprising, since dust clumps at distances $\gtrsim$1 kpc, observed at relatively low angular resolution, may be still large enough to host more than one compact source, possibly in different evolutionary phases. Therefore, an improved analysis of the correlation between maser activity and the physical properties of the gas clump will only be possible through higher angular resolution maps of the molecular gas in the masers' environment.

4.4. OH association

As mentioned in Sect. 3.2 only one of the new methanol masers discovered by us has an associated excited OH maser, when the velocity range of the maser emission is also used as a criterion for the masers to be physically associated. However, if we also include the known methanol masers, then the number of sources with both maser types is 5 out of a total of 37 methanol masers. The main observational property that characterizes the sources where both types of maser activity is present, is the higher intensity of the methanol masers as compared to sources with no OH detection. In fact, Table 5 tentatively suggests (because of the large scatter) that both peak flux density and the flux of methanol maser emission may have higher values on-average in sources associated with an OH maser. Although our sample is relatively small, and the scatter around the average values too large, this result is consistent with the findings of Breen et al. (2010) toward a larger sample of more intense methanol and OH masers. We should note that the situation is not similar when one considers the OH masers (see Table 6). In fact, the median values of the peak flux density of the OH masers is comparable in sources with and without an associated methanol maser. Despite the *caveats* mentioned above, we can discuss our results in the context of maser excitation and compare them to the proposed scenarios of maser evolution.

The model calculations of Cragg et al. (2002) show that the coincidence of OH and methanol masers in many sources can be explained in terms of common excitation conditions that produce population inversions simultaneously in both molecules. The masers require infrared pumping radiation from warm ($T_{\rm d}$ > 100 K) dust and are most likely to form in cooler ($T_{\rm k}$ < 100 K) gas of moderately high density ($10^5 < n_{\rm H} < 10^{8.3}$ cm^{-3}). When methanol and OH masers are detected, it is necessary that both be present in high abundance in the gas phase. When masers of one or more molecules are seen in isolation, Cragg et al. (2002) gives two possible explanations; either the non-masing molecule is not sufficiently abundant or the local conditions produce maser action in the favored molecule alone.

These authors show that the 6.7 GHz methanol maser is excited at relatively lower densities ($n_{\rm H} > 10^4$ cm^{-3}) than is the 6.035 GHz OH line (which requires $n_{\rm H} \gtrsim 10^5$–10^6 cm^{-3}) and is independent of gas density up to $n_{\rm H} \sim 10^8$ cm^{-3}. This indicates that the methanol maser excitation mechanism is predominantly radiative. On the other hand, the excitation of OH is more sensitive to the local density and also extends to higher densities, where the methanol maser is instead subject to collisional quenching. Cragg et al. (2005), however, showed that collisional quenching at high density of the 6.7 GHz methanol maser becomes less probable when new rate coefficients are used. Furthermore, it should be noted that the model calculations

Table 5. Median values of peak and integrated flux density for all detected methanol masers.

All detections		Sources with OH maser		Sources without OH maser	
Median S_{pk} [Jy]	Median $\int S\,dV$ [Jy km s^{-1}]	Median S_{pk} [Jy]	Median $\int S\,dV$ [Jy km s^{-1}]	Median S_{pk} [Jy]	Median $\int S\,dV$ [Jy km s^{-1}]
0.09	0.05	11.4	17.6	0.07	0.04

Table 6. Median values of peak and integrated flux density for all detected OH masers.

All detections		Sources with CH_3OH maser		Sources without CH_3OH maser	
Median S_{pk} [Jy]	Median $\int S\,dV$ [Jy km s^{-1}]	Median S_{pk} [Jy]	Median $\int S\,dV$ [Jy km s^{-1}]	Median S_{pk} [Jy]	Median $\int S\,dV$ [Jy km s^{-1}]
0.04	0.03	0.05	0.07	0.03	0.02

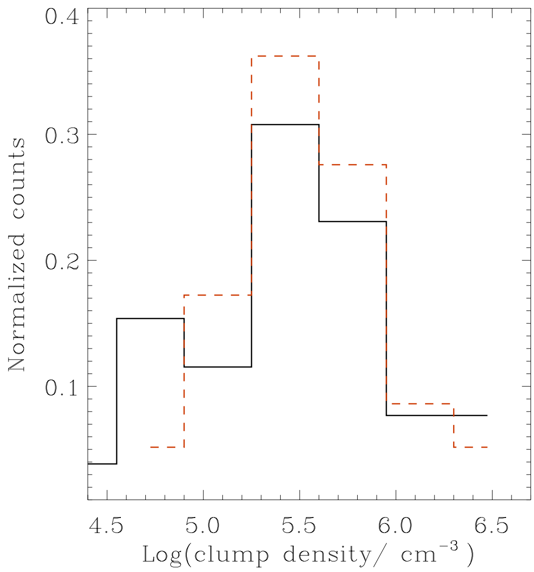

Fig. 11. Density of all observed Hi-GAL clumps in our survey. The black (solid) and red (dashed) lines represent the distribution of sources with and without, respectively, an associated methanol maser.

of Cragg et al. (2002) all refer to emerging masers with a brightness temperature exceeding 10^4 K, or 0.1 Jy for a 6 GHz maser of size 0.7 arcsec. Therefore, their conclusions may not be entirely valid for weaker maser emission.

According to Cragg et al. (2002, 2005), there is therefore a limited range of conditions that favor maser action in just one molecule, and they claim that molecular abundance is likely to be the determining factor of methanol and OH maser activity in HMSF regions. If that is indeed the case, then the presence or absence of both maser types should be able to be tied to the chemical evolution and age of the HMSF region. A common proposed scenario (Cragg et al. 2002; Ellingsen et al. 2011 and references therein) is that the gas-phase methanol abundance is enriched in maser regions following the evaporation of icy grain mantles. The same process is responsible for injecting water molecules in the gas phase, then for leading to the production of OH through photodissociation or ion-molecule chemistry. This is consistent with a time span when both masers are present, but chemical models (e.g., Charnley et al. 1992, 1995) predict that the OH abundance should peak after the methanol abundance has started to diminish (about 10^5 yr after grain mantle molecules have been injected in the gas phase). Therefore, methanol masers are expected to start (and finish) earlier than OH masers.

4.5. IR counterparts

The association between mid-infrared emission and 6.7 GHz methanol masers has already been investigated in several of the previous surveys. Recent works (e.g., Ellingsen 2006; Cyganowski et al. 2009; Pandian et al. 2011) have found a very close correspondence between 6.7 GHz methanol masers and mid-infrared emission, although it should be noted that in some cases (Ellingsen 2006; Cyganowski et al. 2009), these were targeted searches toward GLIMPSE point sources that resulted in high detection rates for 6.7 GHz methanol masers. However, even Pandian et al. (2011) found that almost all AMGPS 6.7 GHz methanol masers had indeed associated an MIPS 24 μm counterpart within 5 arcsec.

We then searched the all-sky data release[6] of the Wide-field Infrared Survey Explorer (WISE, Wright et al. 2010) for counterparts to our Hi-GAL clumps with methanol masers. We found that all (except one) Hi-GAL clumps with maser detection have at least one WISE counterpart within 15 arcsec. Clearly, a more detailed analysis of this association will require mapping the masers (and, ideally, the Hi-GAL clumps as well) at higher angular resolution in order to determine their relative positions within the Hi-GAL clump and also with respect to the WISE 22 μm counterpart(s).

4.6. Correlation between maser intensity and velocity range

Our previous discussion indicates that our blind survey of Hi-GAL sources is more sensitive to the low flux-density methanol masers that have escaped previous surveys. We have also seen in Sect. 4.4 that theoretical models suggest that the presence of a given maser type may be linked with the chemical evolution and age of the HMSF region, although this is difficult to verify observationally without higher angular resolution observations. However, even our observations have shown a peculiar and interesting correlation. In fact, Fig. 9 shows that the brightest masers tend to occur in regions with wide velocity ranges, and vice versa. As discussed in Sect. 3.3, we can tentatively assume that the lack of multiple velocity components toward the less bright masers is not an observational effect of limited sensitivity or positional offsets, but may instead be a consequence of geometrical effects.

In fact, if maser emission were originated only in spherically symmetric cloudlets, then the emitted radiation would be isotropic, though highly beamed in the sense described, e.g., by

[6] `http://wise2.ipac.caltech.edu/docs/release/allsky/expsup/index.html`

Elitzur (1992). However, the conditions in which most masers form are likely to be complex and turbulent, and the individual maser cloudlets will almost certainly be asymmetric. Then, as shown by Alcock & Ross (1985), even a modest elongation of the maser cloud can produce substantial anysotropy of the outgoing radiation. It is thus reasonable to assume that in those regions with relatively few maser spots (and thus with a lower velocity range), we are less likely to observe any (anysotropic) maser emission. However, in regions with many maser spots, the probability that the observer is aligned with the beaming solid angle of one or more velocity components is clearly higher.

Variability of maser emission can be due to both regular and turbulent motions of material with different scales and lifetimes, as well as to variations in the pumping source itself. In addition, maser condensations can split into separate fragments due to interaction with dense material of the medium where the masers are generated (see, e.g., Lekht et al. 2009). The overall evolution of the maser spots and their number is not known, but if the number of maser spots actually *increases* during the evolution of the star-forming region, then our observations are consistent with these weak masers indeed representing an earlier stage.

5. Conclusions

We have observed 107 high-mass dust clumps with the Arecibo telescope in search of the 6.7 GHz methanol and 6.0 GHz excited OH masers. The clumps were selected from the Hi-GAL survey to be relatively massive and visible from Arecibo. We detected a total of 37 methanol masers, where 22 sources are new and weak (median peak flux density 0.07 Jy) detections, in the Galactic longitude range [$32.^{\circ}0$, $59.^{\circ}8$].

We have compared our results with previous similar surveys, in particular with the "Arecibo Methanol Maser Galactic Plane Survey" (Pandian et al. 2007), and found that although both source samples approximately cover the same distance range, our newly discovered masers are clearly shifted toward much lower integrated flux densities compared to the AMGPS. Using five-pointing cross scans, we checked, in a subsample of sources, if the masers were being observed off-peak. In most cases, the resulting maser peak positions turned out to be very close (i.e., within the Arecibo pointing error) to the pointed positions, i.e. the nominal positions of the Hi-GAL sources. Thus, most of the methanol masers observed toward our Hi-GAL massive dust clumps appear to be intrinsically weaker than previously observed masers in unbiased surveys.

While the better sensitivity and the sample used in our observations have allowed us to detect lower flux density methanol masers compared to previous unbiased surveys, the physical reasons determining these intrinsically lower intensities still have to be determined. We found no statistically significant correlation with the physical parameters of the Hi-GAL clumps, except possibly for sources with both maser types that appear to have higher mass and luminosity than do sources with just one type of maser emission. The merged luminosity function of the methanol masers detected by us and the AMGPS shows an essentially flat distribution for luminosities between $\sim 10^{-7}$ and $\sim 10^{-5}$ $L_{\odot}$ and a relatively quick drop outside of this range. The intensity of the methanol masers correlates well with the velocity range of the maser emission, which suggests that the low brightness of these masers is related to the number of maser spots in the emitting region and their evolution with time.

Acknowledgements. We wish to thank the staff of the Arecibo Observatory for the support provided before and during the observations. P.H. acknowledges support from NSF grant AST-0908901.

References

Alcock, C., & Ross, R. R. 1985, ApJ, 290, 433
Breen, S. L., Caswell, J. L., Ellingsen, S. P., & Phillips, C. J. 2010, MNRAS, 406, 1487
Brunthaler, A., Reid, M. J., Menten, K. M., et al. 2011, Astron. Nachr., 332, 461
Caswell, J. L., & Vaile, R. A. 1995, MNRAS, 273, 328
Caswell, J. L., Vaile, R. A., Ellingsen, S. P., Whiteoak, J. B., & Norris, R. P. 1995, MNRAS, 272, 96
Charnley, S. B., Kress, M. E., Tielens, A. G. G. M., & Millar, T. J. 1995, ApJ, 448, 232
Charnley, S. B., Tielens, A. G. G. M., & Millar, T. J. 1992, ApJ, 399, L71
Cragg, D. M., Sobolev, A. M., & Godfrey, P. D. 2002, MNRAS, 331, 521
Cragg, D. M., Sobolev, A. M., & Godfrey, P. D. 2005, MNRAS, 360, 533
Cyganowski, C. J., Brogan, C. L., Hunter, T. R., & Churchwell, E. 2009, ApJ, 702, 1615
Elia, D., Schisano, E., Molinari, S., et al. 2010, A&A, 518, L97
Elia, D., Molinari, S., Fukui, Y., et al. 2013, ApJ, 772, 45
Elitzur, M. 1992, ARA&A, 30, 75
Ellingsen, S. P. 2006, ApJ, 638, 241
Ellingsen, S. P., Breen, S. L., Sobolev, A. M., et al. 2011, ApJ, 742, 109
Green, J. A., Caswell, J. L., Fuller, G. A., et al. 2008, MNRAS, 385, 948
Green, J. A., Caswell, J. L., Fuller, G. A., et al. 2009, MNRAS, 392, 783
Green, J. A., Caswell, J. L., Fuller, G. A., et al. 2010, MNRAS, 409, 913
Green, J. A., & McClure-Griffiths, N. M. 2011, MNRAS, 417, 2500
Hill, T., Burton, M. G., Minier, V., et al. 2005, MNRAS, 363, 405
Hoare, M. G., Purcell, C. R., Churchwell, E. B., et al. 2012, PASP, 124, 939
Jackson, J. M., Rathborne, J. M., Shah, R. Y., et al. 2006, ApJS, 163, 145
Lekht, E. E., Silant'ev, N. A., & Alekseeva, G. A. 2009, Astron. Rep., 53, 813
Menten, K. M. 1991, ApJ, 380, L75
Molinari, S., Swinyard, B., Bally, J., et al. 2010, PASP, 122, 314
Olmi, L., Anglés-Alcázar, D., Elia, D., et al. 2013, A&A, 551, A111
Pandian, J. D., & Goldsmith, P. F. 2007, ApJ, 669, 435
Pandian, J. D., Goldsmith, P. F., & Deshpande, A. A. 2007, ApJ, 656, 255
Pandian, J. D., Menten, K. M., & Goldsmith, P. F. 2009, ApJ, 706, 1609
Pandian, J. D., Momjian, E., Xu, Y., Menten, K. M., & Goldsmith, P. F. 2011, ApJ, 730, 55
Pestalozzi, M. 2012, in IAU Symp. 287, eds. R. S. Booth, W. H. T. Vlemmings, & E. M. L. Humphreys, 492
Pestalozzi, M., Humphreys, E. M. L., & Booth, R. S. 2002, A&A, 384, L15
Pestalozzi, M. R., Minier, V., & Booth, R. S. 2005, A&A, 432, 737
Pestalozzi, M. R., Chrysostomou, A., Collett, J. L., et al. 2007, A&A, 463, 1009
Purcell, C. R., Hoare, M. G., Cotton, W. D., et al. 2013, ApJS, 205, 1
Reach, W. T., Rho, J., & Jarrett, T. H. 2005, ApJ, 618, 297
Reid, M. J., Menten, K. M., Zheng, X. W., et al. 2009, ApJ, 700, 137
Russeil, D. 2003, A&A, 397, 133
Russeil, D., Pestalozzi, M., Mottram, J. C., et al. 2011, A&A, 526, A151
Schneider, N., Bontemps, S., Simon, R., et al. 2011, A&A, 529, A1
Slysh, V. I., Val'tts, I. E., Kalenskii, S. V., et al. 1999, A&AS, 134, 115
Szymczak, M., & Gérard, E. 2004, A&A, 414, 235
Szymczak, M., Hrynek, G., & Kus, A. J. 2000, A&AS, 143, 269
Szymczak, M., Kus, A. J., Hrynek, G., Kěpa, A., & Pazderski, E. 2002, A&A, 392, 277
van der Walt, J. 2005, MNRAS, 360, 153
Walsh, A. J., Hyland, A. R., Robinson, G., & Burton, M. G. 1997, MNRAS, 291, 261
Wright, E. L., Eisenhardt, P. R. M., Mainzer, A. K., et al. 2010, AJ, 140, 1868

Pages 13 to 16 are available in the electronic edition of the journal at http://www.aanda.org

Appendix A: Spectra of methanol masers

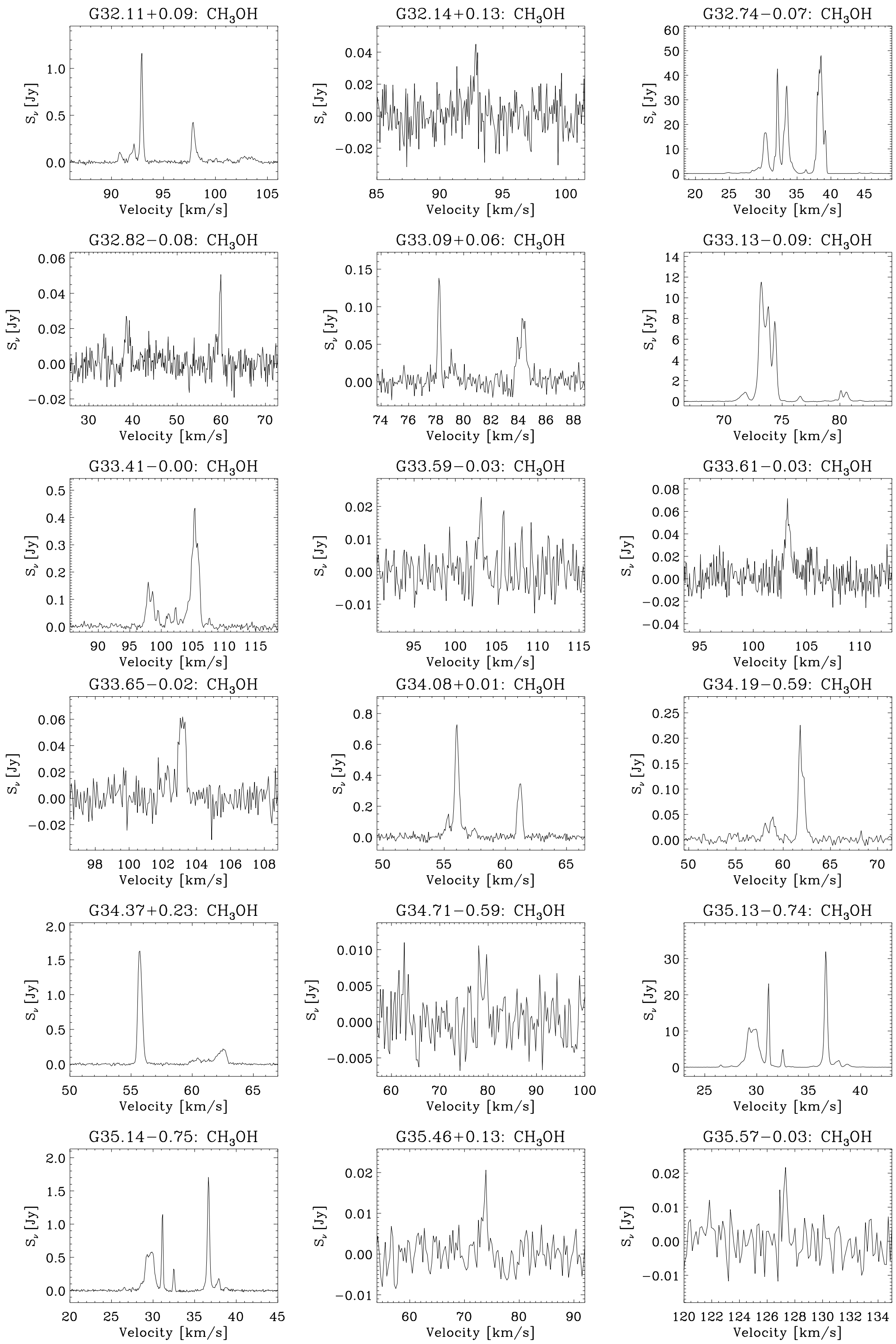

Fig. A.1. Spectra of methanol masers.

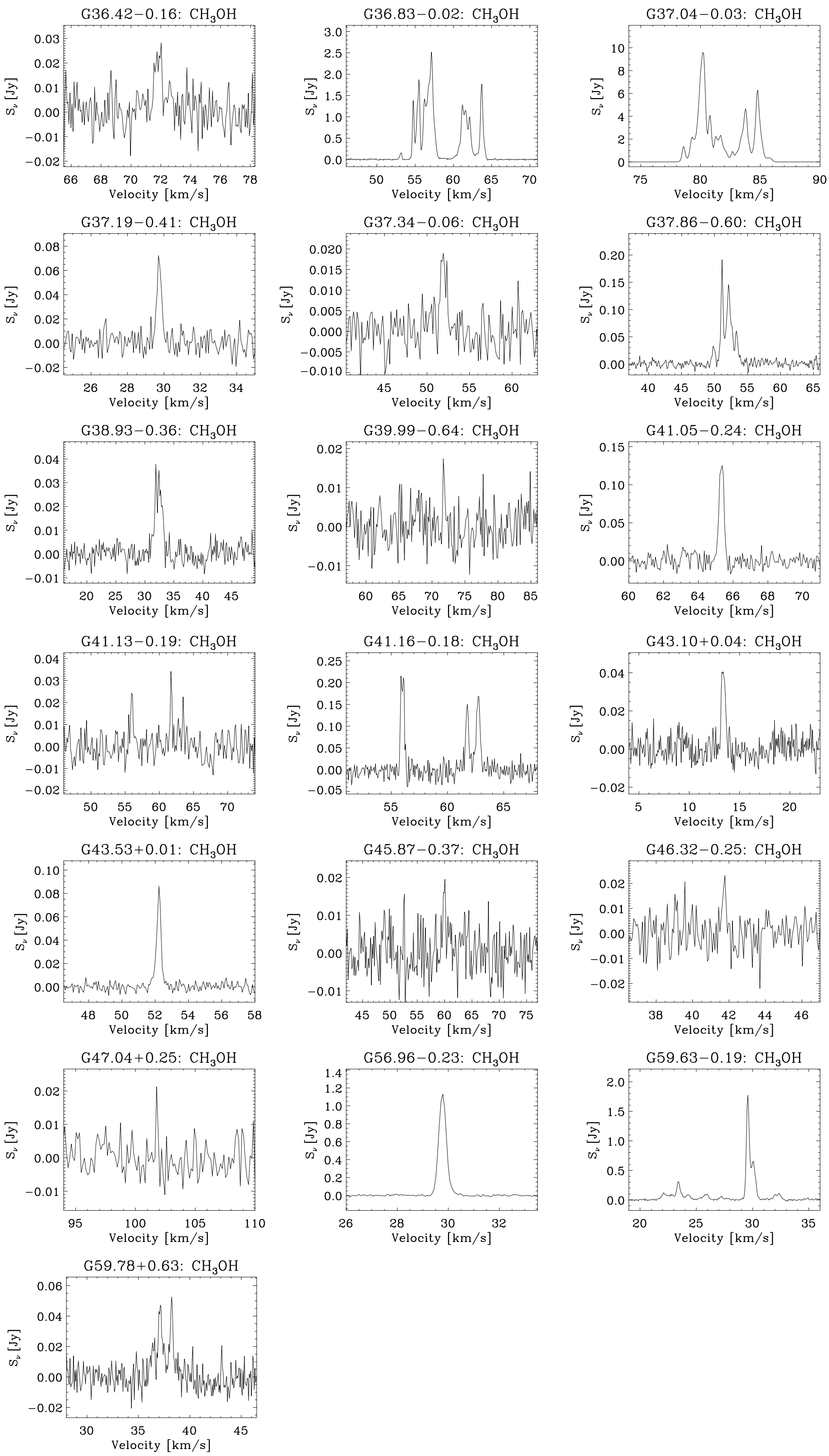

Fig. A.1. continued.

Appendix B: Spectra of OH masers

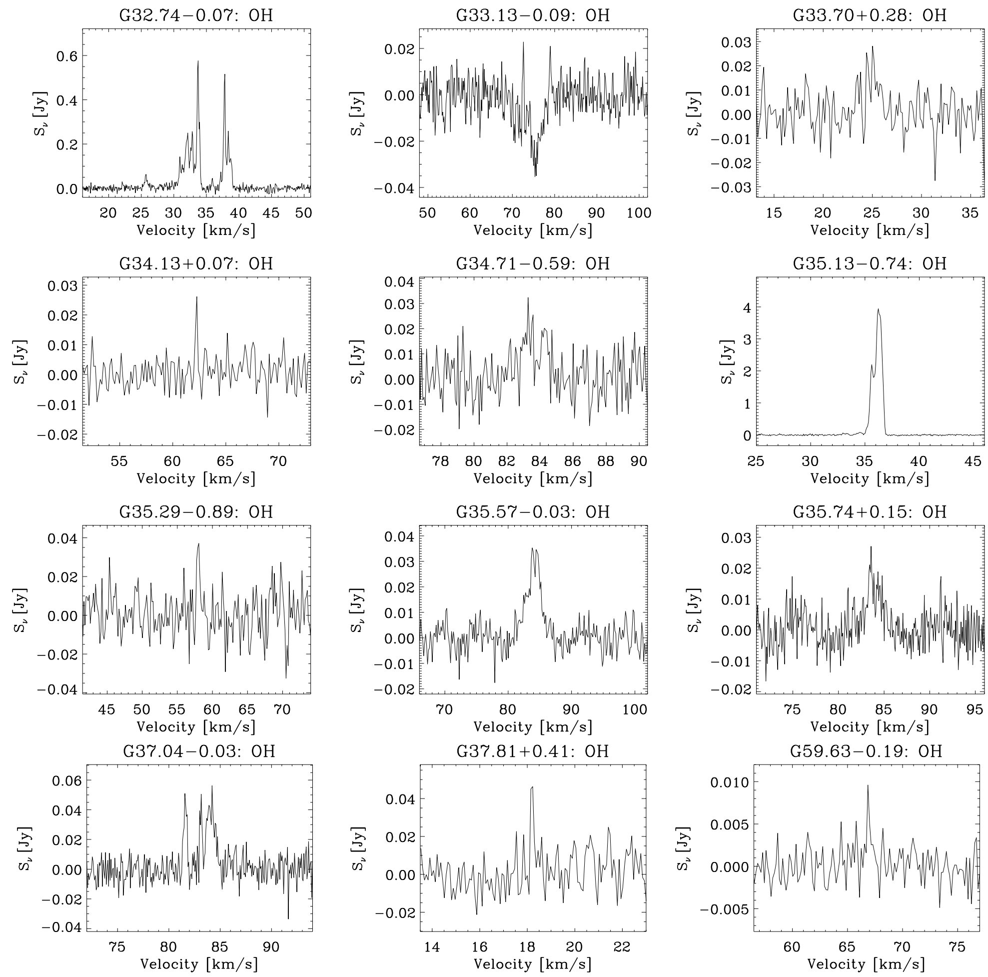

Fig. B.1. Spectra of OH masers.

Appendix C: Sources with no methanol detection

Table C.1. Hi-GAL sources with no detection of 6.7 GHz methanol masers.

Name	RA [J2000.0]	Dec [J2000.0]	rms [mJy]
G32.45+0.38	18:49:11.6	–00:14:49	6
G32.45+0.15	18:50:00.2	–00:21:21	10
G32.03-0.32	18:50:58.1	–00:56:54	10
G33.11+0.06	18:51:33.3	00:11:43	10
G32.98-0.07	18:51:47.4	00:00:38	9
G33.26+0.06	18:51:48.4	00:19:37	10
G33.70+0.28	18:51:50.4	00:49:05	14
G33.71+0.25	18:51:57.1	00:48:48	9
G33.49-0.01	18:52:30.8	00:29:47	10
G33.02-0.36	18:52:54.6	–00:05:05	10
G34.46+0.24	18:53:20.5	01:28:26	9
G34.13+0.07	18:53:21.3	01:06:11	9
G33.33-0.53	18:54:03.9	00:06:55	9
G34.00-0.29	18:54:26.5	00:49:32	10
G35.42+0.43	18:54:27.2	02:24:52	9
G34.94+0.15	18:54:33.2	01:51:59	9
G34.69+0.00	18:54:39.2	01:34:22	9
G34.24-0.26	18:54:46.7	01:02:46	9
G34.93+0.01	18:55:01.1	01:47:23	9
G35.56+0.10	18:55:53.1	02:23:24	9
G35.60+0.10	18:55:56.1	02:25:58	9
G35.74+0.15	18:56:01.0	02:34:34	8
G35.44-0.00	18:56:03.1	02:13:49	10
G35.61-0.07	18:56:36.8	02:21:20	9
G35.68-0.17	18:57:04.9	02:21:59	8
G35.52-0.27	18:57:08.3	02:10:53	9
G36.40+0.02	18:57:42.0	03:06:07	9
G37.49+0.53	18:57:53.3	04:18:18	8
G36.45-0.18	18:58:31.4	03:03:01	9
G37.17+0.10	18:58:49.6	03:49:15	5
G37.61+0.31	18:58:51.5	04:18:33	11
G37.81+0.41	18:58:53.9	04:32:15	9
G35.29-0.89	18:58:57.0	01:41:40	18
G37.42+0.13	18:59:09.4	04:03:38	9
G37.37-0.23	19:00:23.7	03:50:38	9
G38.19-0.15	19:01:35.9	04:36:43	7
G38.42-0.16	19:02:04.6	04:48:24	8
G38.32-0.22	19:02:06.1	04:42:01	8
G39.25-0.05	19:03:12.8	05:35:51	10
G38.69-0.45	19:03:35.2	04:55:06	10
G38.92-0.41	19:03:52.9	05:08:12	7
G39.49-0.20	19:04:10.5	05:44:55	9
G38.35-0.95	19:04:44.8	04:23:18	8
G39.85-0.21	19:04:53.1	06:03:44	10
G39.26-0.58	19:05:07.9	05:22:00	8
G39.36-0.56	19:05:13.9	05:27:34	8
G40.36-0.05	19:05:15.7	06:34:52	8
G43.23-0.04	19:10:33.5	09:08:25	8
G42.15-0.66	19:10:45.5	07:53:43	9
G43.51+0.01	19:10:51.6	09:25:01	9
G42.23-0.65	19:10:53.3	07:58:23	9
G43.30-0.21	19:11:16.9	09:07:29	8
G43.32-0.20	19:11:17.4	09:08:48	8
G44.48-0.13	19:13:12.9	10:12:20	10
G44.49-0.15	19:13:17.5	10:12:08	10
G45.95+0.07	19:15:14.4	11:36:17	9
G47.09-0.27	19:16:42.2	12:42:27	7
G45.38-0.74	19:17:07.5	10:43:09	10
G45.88-0.51	19:17:14.0	11:16:18	7
G46.42-0.23	19:17:16.8	11:52:31	8
G46.17-0.52	19:17:49.1	11:31:03	4
G47.00-0.26	19:18:28.6	12:22:36	5
G54.45+1.01	19:28:25.8	19:32:33	7
G54.39+0.92	19:28:38.0	19:26:51	7
G54.11-0.08	19:31:48.7	18:42:58	7
G54.22-0.11	19:32:10.6	18:47:52	7
G55.74+0.11	19:34:27.2	20:14:33	8
G55.15-0.29	19:34:45.9	19:31:39	5
G56.06-0.12	19:36:00.0	20:24:08	7
G56.89-0.18	19:37:58.4	21:05:55	9

Notes. The last column lists the rms (in mJy) of the final spectrum.